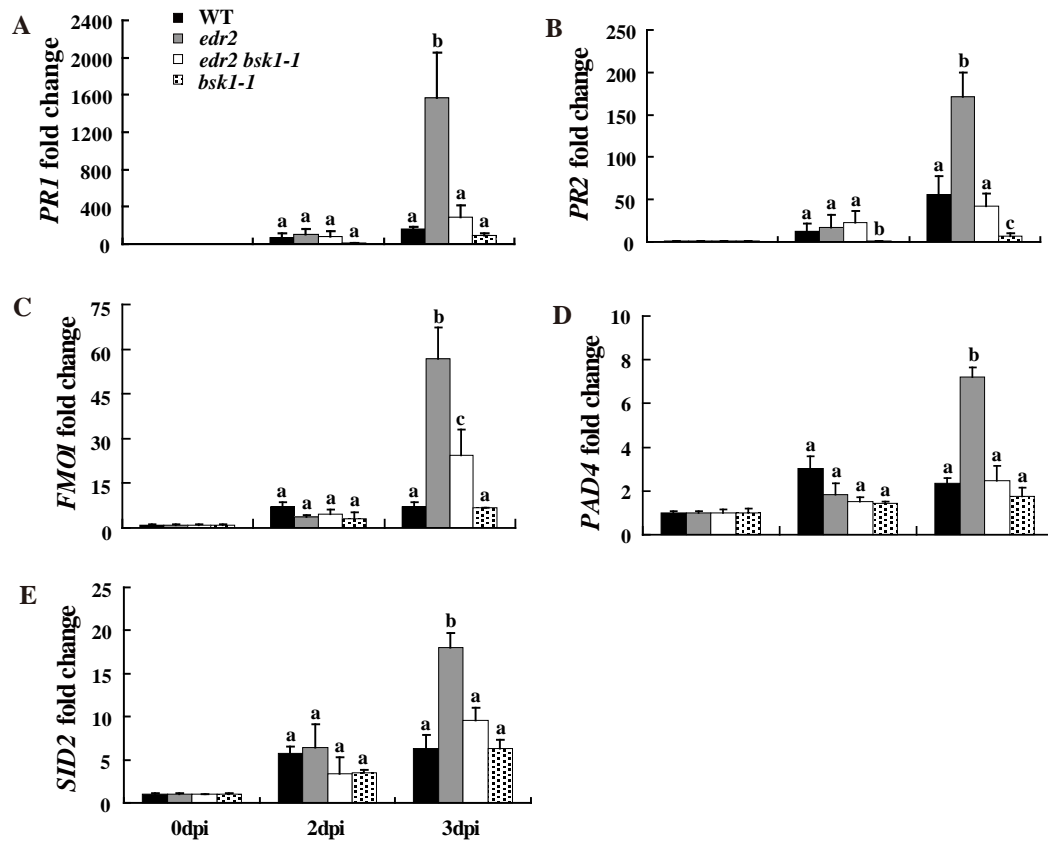


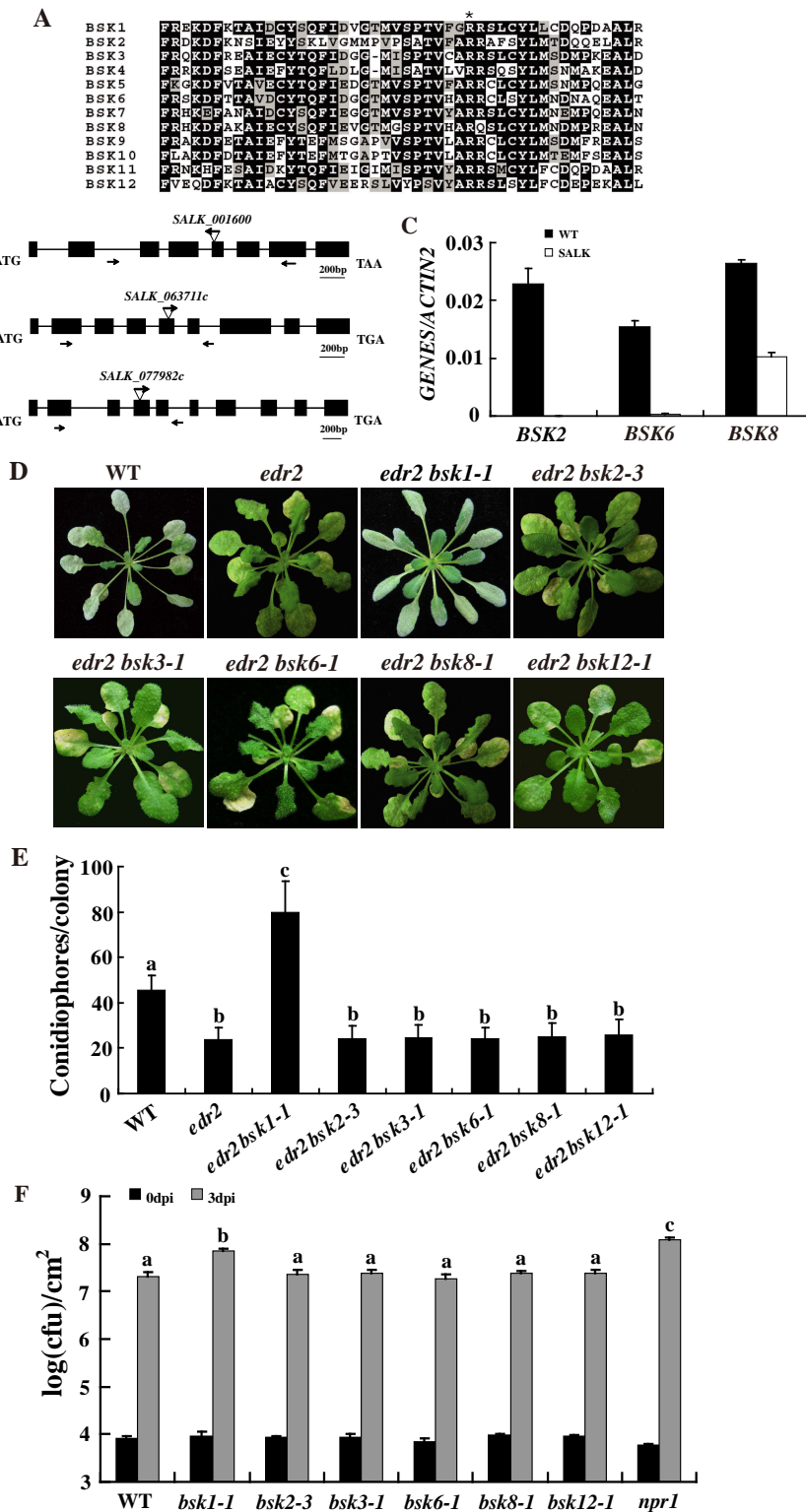
Supplemental Figure 1



Supplemental Figure 1. *bsk1-1* affects *edr2*-mediated changes in gene expression.

The transcript accumulation of defense-related genes were examined by quantitative real-time PCR. Leaves were detached from plants for RNA isolation at different time points (day 0, 2 and 3) after infection with *G. cichoracearum*. (A) *PR1*, (B) *PR2*, (C) *FMO1*, (D) *PAD4*, (E) *SID2*. The relative fold change of transcript accumulation was calculated relative to uninoculated control plants (day 0) at the indicated time points. Bars represent standard deviation of values obtained from three independent biological samples per genotype and time point. Three technical replicates per biological samples were also examined in the experiment. Lower-case letters indicate statistically significant differences (P<0.05; one-way ANOVA). WT, wild type.

Supplemental Figure 2



Supplemental Figure 2. T-DNA insertion mutations of *BSK1* homologs did not suppress *edr2*-mediated powdery mildew resistance, and mutants of *BSK1* homologs displayed wild type like responses to *Pto* DC3000.

(A) Alignment of the BSK1 TPR domain with the most similar BSK1 homologs in Arabidopsis. The mutation site (asterisk) of *bsk1-1* (R443) is highly conserved in the BSK1 protein family.

(B) T-DNA insertion sites are indicated by arrows and triangles. The positions of the primers used to examine transcript levels were indicated by arrows.

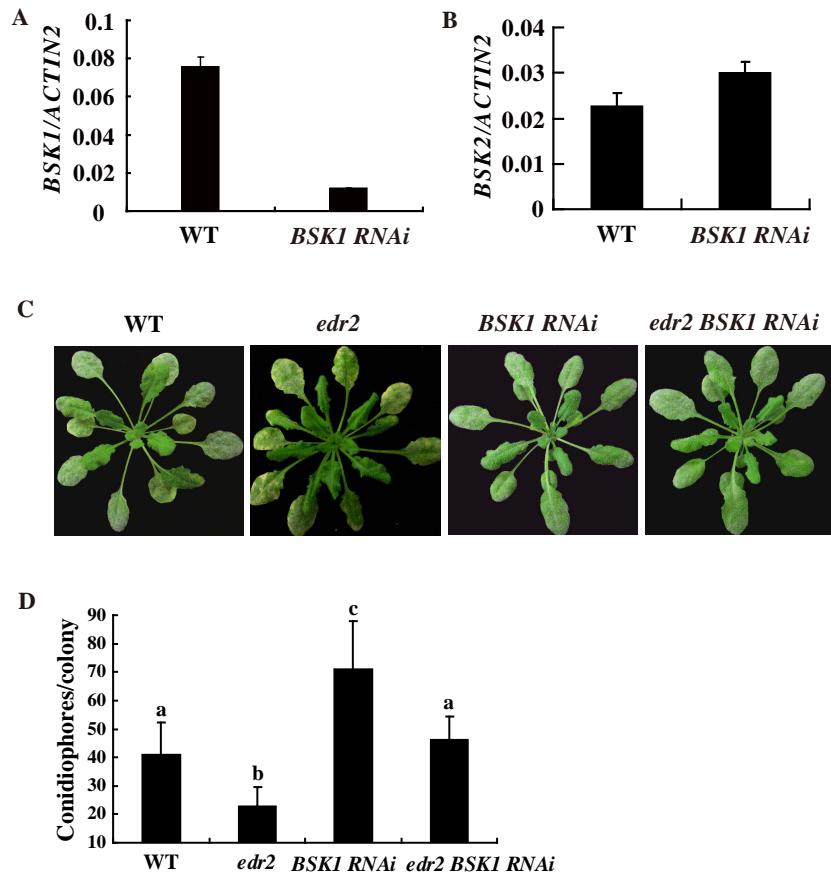
(C) Relative expression levels were examined by Real time PCR. *ACTIN2* was used as the internal control. Error bars represent standard deviation of values obtained from three independent biological samples.

(D) Four-week-old plants of the indicated genotypes were inoculated with *G. cichoracearum* and photographed at 8 dpi.

(E) The number of conidiophores per colony was counted at 5 dpi. Bars represent mean and standard deviation (n>30). Statistically significant differences are indicated by lower-case letters (P<0.01; one-way ANOVA). Experiments were repeated three times with similar results.

(F) Four-week-old plants were inoculated with 5×10^5 cfu/ml of *Pto* DC3000. The bacterial growth was counted at 3 dpi. Statistically significant differences are indicated by lower-case letters (P<0.01, one-way ANOVA). The experiments were repeated three times with similar results.

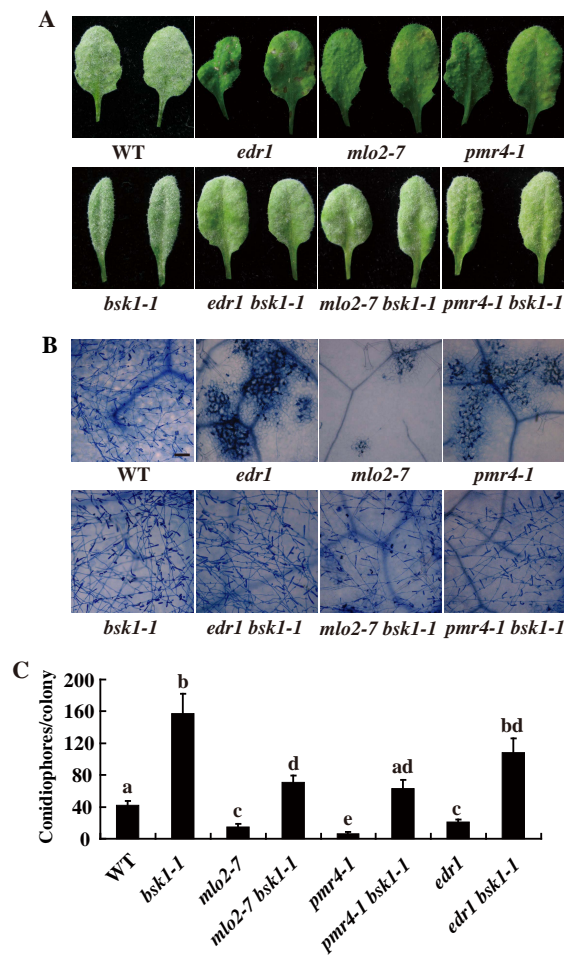
Supplemental Figure 3



Supplemental Figure 3. *BSK1 RNAi* lines displayed a similar phenotype to *bsk1-1*.

- (A) The accumulation of *BSK1* transcripts in *BSK1 RNAi* T2 lines was examined by quantitative Real-time PCR. *ACTIN2* was used as the internal control. Error bars represent standard deviation of values obtained from three independent biological samples. WT, wild type.
- (B) Accumulation of *BSK2* transcripts was examined by quantitative real time PCR. *ACTIN2* was used as the internal control. Error bars represent standard deviation of values obtained from three independent biological samples. The expression levels of *BSK2* in *BSK1 RNAi* transgenic plants were similar to those in wild-type plants, indicating that the *BSK1 RNAi* construct was specific to *BSK1*.
- (C) Four-week-old plants were inoculated with *G. cichoracearum* and photographed at 8 dpi.
- (D) The number of conidiophores per colony in the infected leaves was counted at 5 dpi. Bars represent mean and standard deviation (n>30). Lower-case letters indicate statistically significant differences (P<0.01; one-way ANOVA). Experiments were repeated three times with similar results.

Supplemental Figure 4



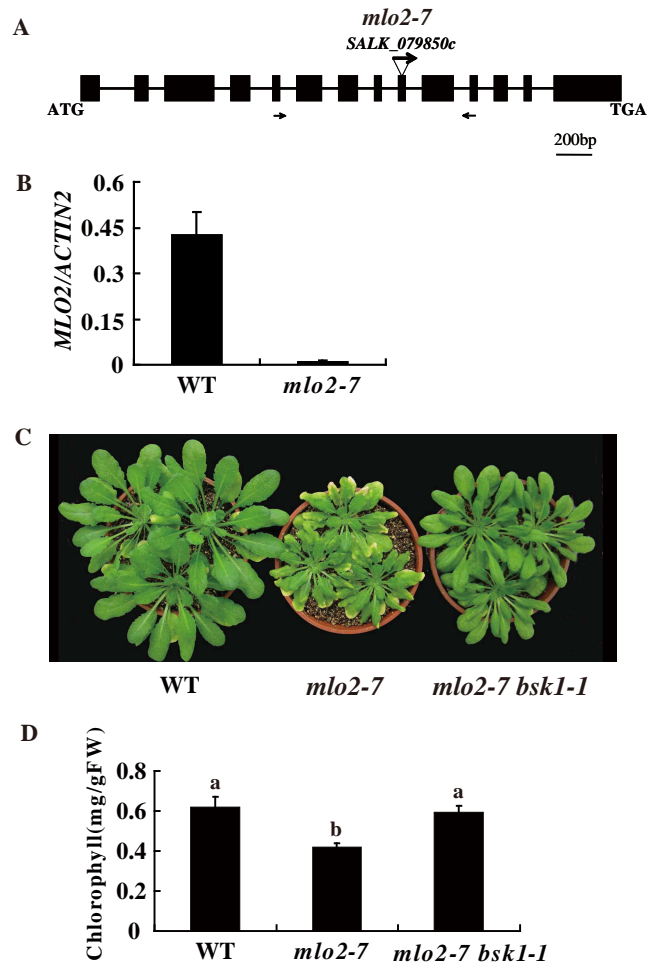
Supplemental Figure 4. The *bsk1-1* mutation suppresses *edr1* and *pmr4*, *mlo2*-mediated powdery mildew resistance phenotypes.

(A) Four-week-old plants were infected with *G. cichoracearum*. Leaves were detached and photographed at 8 dpi. The *edr1*, *pmr4* and *mlo2* mutants were resistant and displayed mildew-induced cell death, but the *edr1 bsk1-1*, *pmr4 bsk1-1* and *mlo2 bsk1-1* mutants showed abundant conidiophores and lacked necrotic lesions. WT, wild type.

(B) Fungal structures on the surface of leaves and dead plant cells at 8 dpi were visualized by trypan blue staining. Very few fungal spores were produced on *edr1*, *pmr4* and *mlo2*, but a large number of conidia were produced on *edr1 bsk1-1*, *pmr4 bsk1-1* and *mlo2 bsk1-1*. Bar=100 μ m.

(C) Quantitative assessment of fungal growth in plants as indicated in (A) by counting the number of conidiophores per colony at 5 dpi. Data represent mean and standard deviation (n>30). Significant differences are indicated by lower case letters (P< 0.01; one-way ANOVA). The experiments were repeated three times with similar results.

Supplemental Figure 5



Supplemental Figure 5. The *bsk1-1* mutation partially suppresses *mlo2*-mediated senescence.

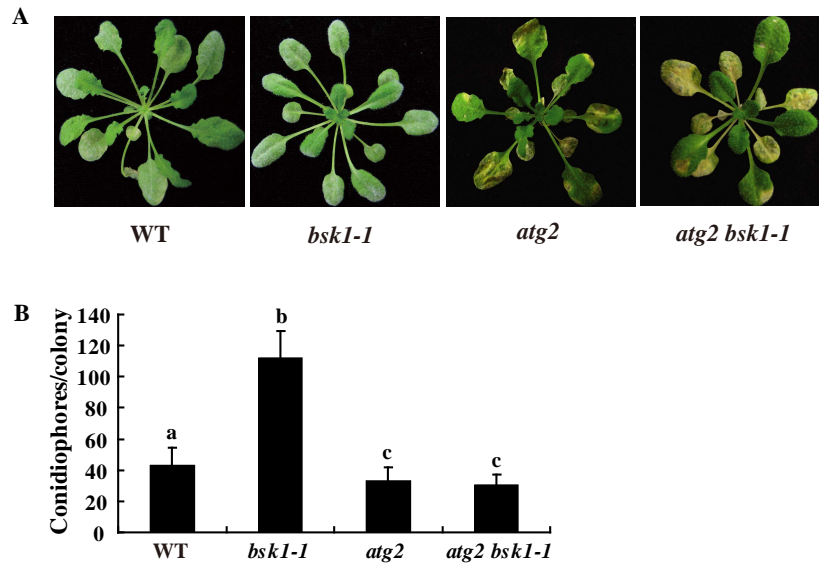
(A) The T-DNA insertion site in the *mlo2-7* mutant is indicated by an arrow and triangle. The positions of the primers used to check transcript levels were indicated by arrows.

(B) The accumulation of *MLO2* transcript was examined by quantitative real time PCR. *ACTIN2* was used as the internal control. Error bars represent standard deviation of values obtained from three independent biological samples. WT, wild type.

(C) Eight-week-old plants grown under standard short-day growth conditions were photographed.

(D) Quantification of chlorophyll content in leaves of the genotype shown in (C). Data represent mean and standard deviation (n=3). Lower case letters indicate statistically significant differences (P< 0.01; one-way ANOVA). The experiments were repeated three times with similar results.

Supplemental Figure 6

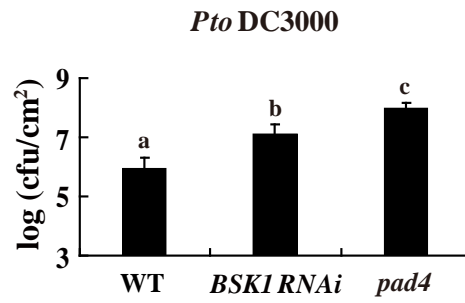


Supplemental Figure 6. The *bsk1-1* mutation did not suppress *atg2*-mediated powdery mildew resistance and cell death phenotypes.

(A) Four-week-old plants were infected with *G. cichoracearum* and photographed at 8 dpi. WT, wild type.

(B) Quantification of fungal growth of the genotype shown in (A) by counting the number of conidiophores per colony at 5 dpi. Bars represent mean and standard deviation (n>30). Statistically significant differences are indicated by lower case letters (P< 0.01; one-way ANOVA). Experiments were repeated three times with similar results.

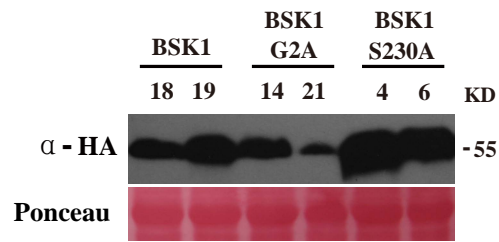
Supplemental Figure 7



Supplemental Figure 7. The *BSK1 RNAi* plants displayed enhanced susceptibility to *Pto* DC3000.

Four-week-old plants were inoculated with 5×10^5 cfu/ml of *Pto* DC3000 and bacterial growth was measured at 3 dpi. Statistically significant differences are indicated by lower case letters ($P < 0.01$; one-way ANOVA). The experiments were repeated three times with similar results. WT, wild type.

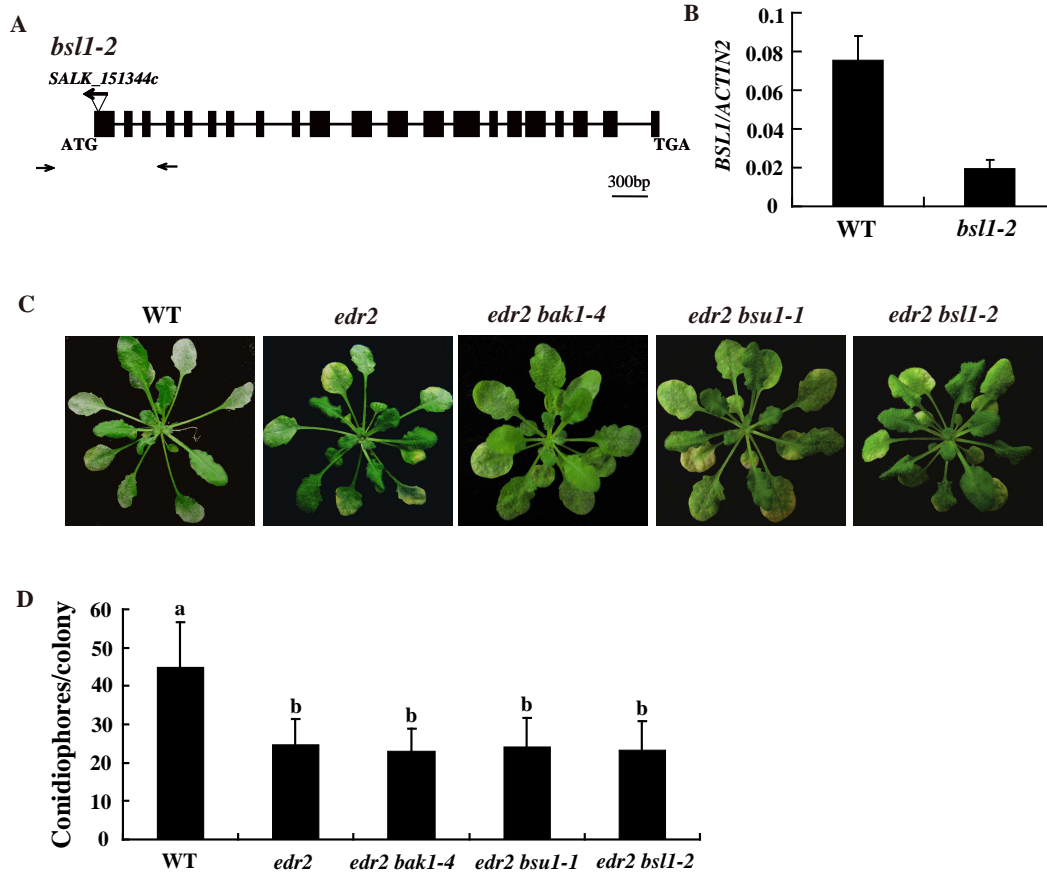
Supplemental Figure 9



Supplemental Figure 9. Transgenic plants expressed correct-sized fusion proteins.

Total protein was extracted from leaves of four-week-old plants. The total protein was separated by SDS-PAGE gel and subjected to immunoblot analysis with anti-HA antibody (upper panel). Ponceau S staining of Rubisco is shown as a loading control (lower panel).

Supplemental Figure 10



Supplemental Figure 10. The *bak1*, *bsu1* and *bslI* mutations did not suppress *edr2*-mediated powdery mildew resistance phenotypes.

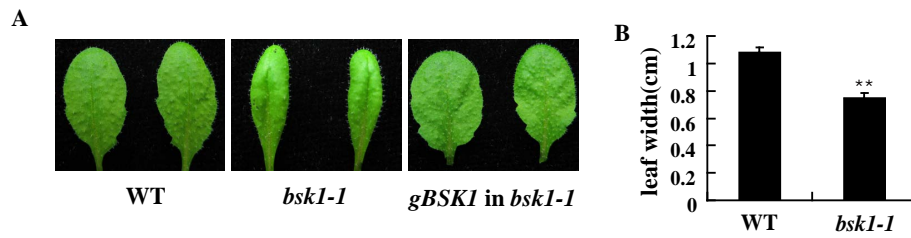
(A) The T-DNA insertion site in *bslI-2* is indicated by an arrow and triangle. The positions of the primers used to check transcript levels were indicated by arrows.

(B) The accumulation of *BSL1* transcripts in *bslI-2* was examined by quantitative real-time PCR. *ACTIN2* was used as the internal control. Error bars represent standard deviation of values obtained from three independent biological samples. WT, wild type.

(C) Four-week-old plants were infected with powdery mildew pathogen *G. cichoracearum* and the plants were photographed at 8 dpi. WT, wild type.

(D) The number of conidiophores per colony on the infected leaves was calculated at 5 dpi. Bars represent mean and standard deviation (n>30). Statistically significant differences among samples are indicated by lower-case letters (P<0.01; one-way ANOVA). Experiments were repeated three times with similar results.

Supplemental Figure 11



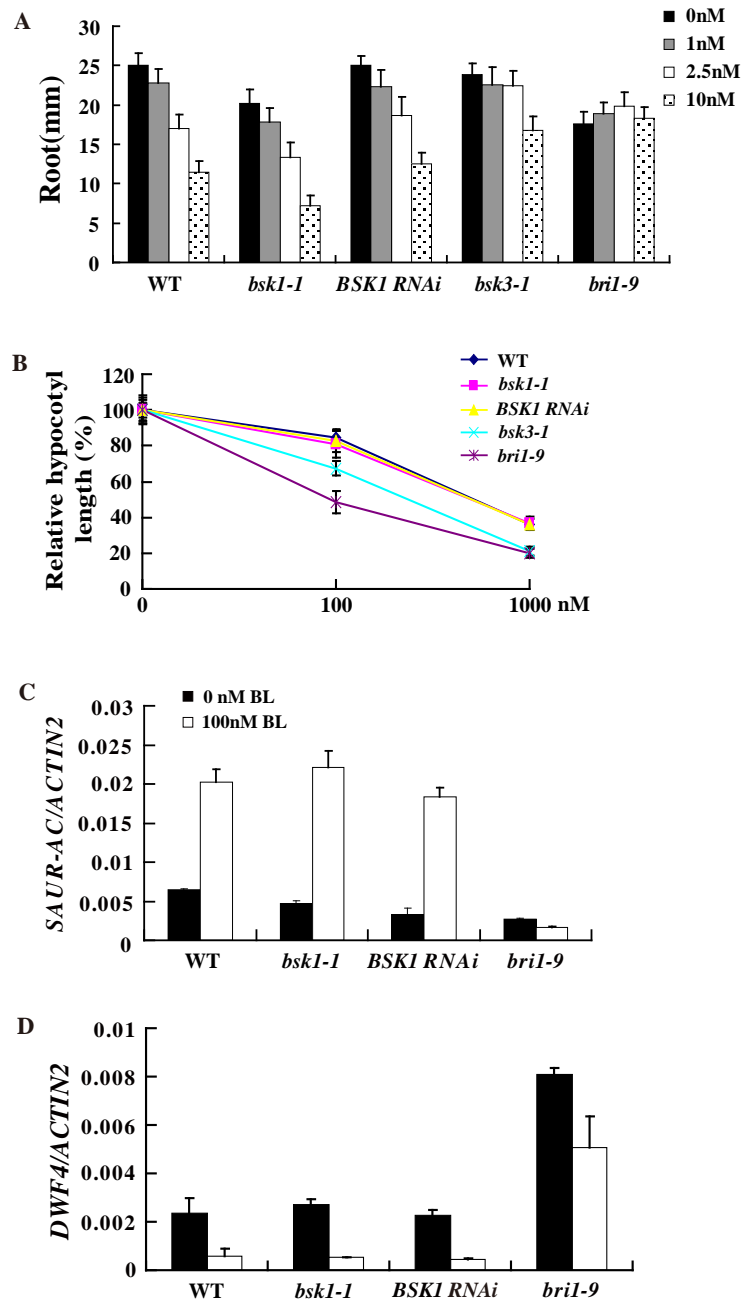
Supplemental Figure 11. The *bsk1-1* mutant displayed a narrow leaf phenotype.

(A) Leaves from four-week-old plants grown under standard short-day growth conditions were photographed.

(B) Four-week-old plants were measured for leaf width. Bars represent mean and standard deviation of data derived from samples (n=40).

(**P< 0.01; Student's *t*-test).

Supplemental Figure 12

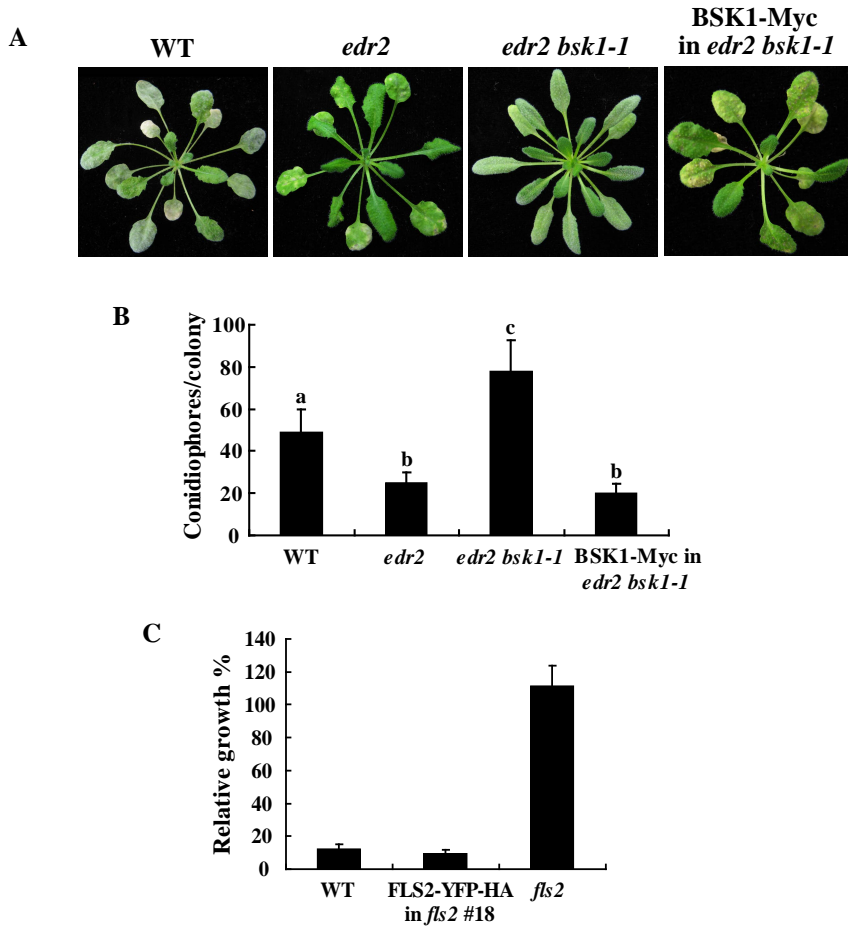
Supplemental Figure 12. *bsk1-1* displayed wild type like responses to BL treatment.

(A) Root growth inhibition by BL at indicated concentrations. Wild type, *bsk1-1*, *BSK1 RNAi*, *bsk3-1* and *bri1-9* seedlings were treated with BL for 7 d, and the root length was measured. Data represent mean and standard deviation (n=30). The experiments were repeated three times with similar results. WT, wild type.

(B) Hypocotyl length inhibition by Brassinazole (BRZ). Seedlings grown in the dark were treated with 100 nM or 1 μ M BRZ for 4 days, and the hypocotyl length was measured. Data represent mean and standard deviation obtained from samples (n=30). Experiments were repeated three times with similar results.

(C) and (D) Expression of *SUAR-AC* (C) or *DARF4* (D) in wild type, *bsk1-1*, *BSK1 RNAi* and *bri1-9* seedlings treated with BL. Seedlings were grown on 1/2 MS for 5 days and treated with 0 or 100 nM BL for 2 h. Transcript levels were normalized to internal control *ACTIN2*. Data represent mean and standard deviation from three independent experiments.

Supplemental Figure 13



Supplemental Figure 13. The BSK1-Myc and FLS2-YFP-HA proteins are functional.

(A) Four-week-old Arabidopsis plants were infected with *G. cichoracearum*. The plants were photographed at 8 dpi. The *BSK1-Myc* clone complemented *bsk1-1* phenotype. WT, wild type.

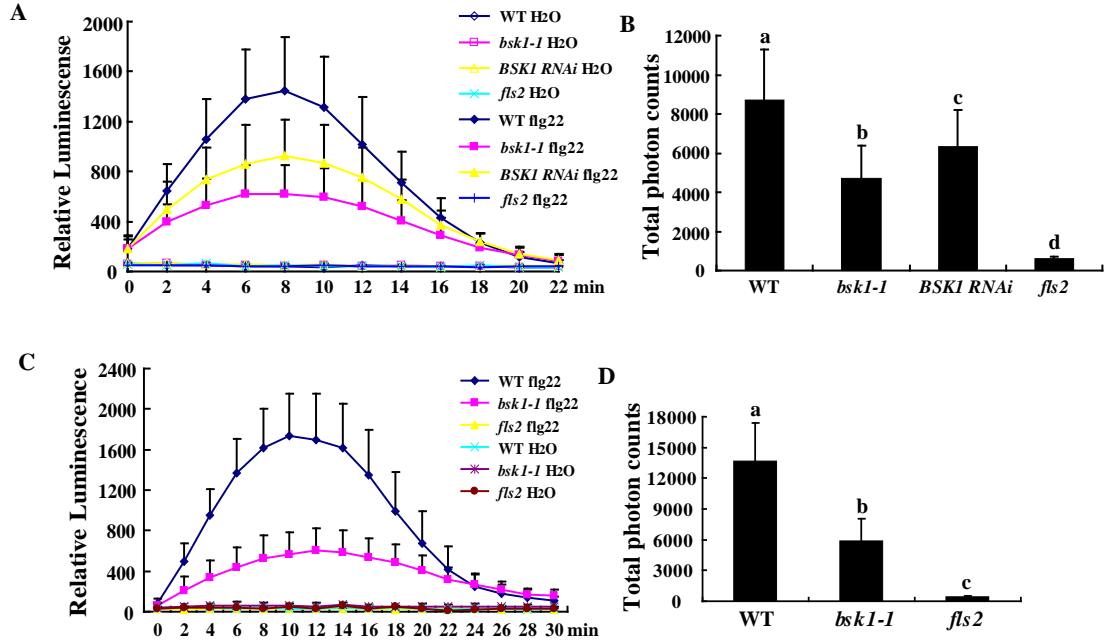
(B) The number of conidiophores per colony was counted at 5 dpi. Bars represent mean and standard deviation of data (n>30). Statistically significant differences are indicated by lower-case letters (P< 0.01; one-way ANOVA). The experiments were repeated three times with similar results.

(C) The *FLS2-YFP-HA* clone complemented *fls2*-mediated flg22 insensitive phenotype. Five-day-old seedlings were treated with 100 nM flg22 for 10 days.

Data represent mean and standard deviation (n=12). WT, wild type.

The experiments were repeated three times with similar results.

Supplemental Figure 14



Supplemental Figure 14. The *BSK1 RNAi* plants showed defects in flg22-induced ROS burst. The *bsk1-1* plants also showed defects in ROS burst when a higher concentration flg22 was used.

(A) Leaves of the wild type, *bsk1-1*, and *BSK1 RNAi* plants were treated with 100 nM flg22, and luminescence was documented at different time points. Bars represent mean and standard deviation obtained from samples (n=12). WT, wild type

(B) ROS production was shown by total photon counts during 30 min treatment.

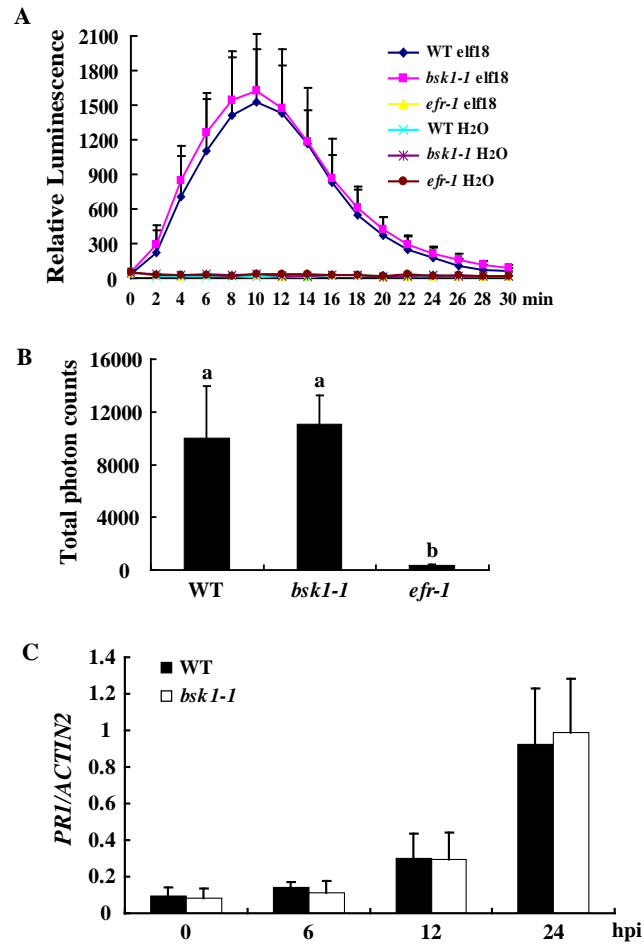
(C) Leaves of the *bsk1-1* plants were treated with 1 μM flg22. Luminescence was recorded at different time points. Bars represent mean and standard deviation (n=12).

(D) ROS production was indicated by total photon counts during 30 min treatment.

(B) and (D) Bars represent mean and standard deviation of data (n=12). Lower-case letters indicate statistically significant differences (P< 0.01; one-way ANOVA).

The experiments were repeated three times with similar results.

Supplemental Figure 15



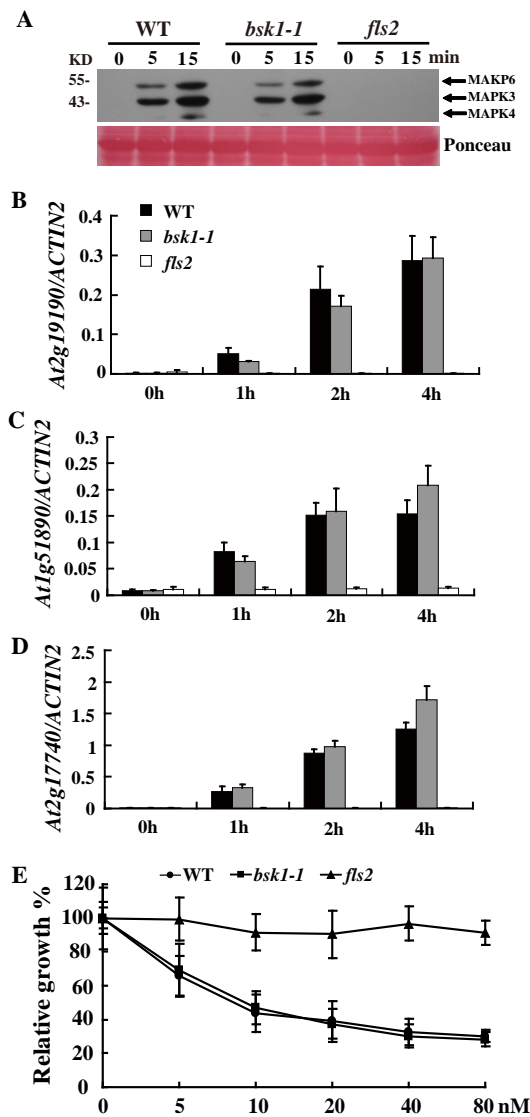
Supplemental Figure 15. The *bsk1-1* plants showed wild type like responses in elf18-induced ROS burst and *PR1* accumulation.

(A) Leaves of wild type, *bsk1-1* and *efr-1* were treated with 1 μ M elf18. Luminescence was recorded at different time points. Bars represent mean and standard deviation (n=12).

(B) ROS production was indicated with total photon counts during 30 min of treatment. Bars represent mean and standard deviation (n=12; P < 0.01, one-way ANOVA).

(C) *PR1* accumulation was examined by quantitative real-time PCR after treatment with 1 μ M elf18. *ACTIN2* was used as an internal control. Bars represent mean and standard deviation from three independent experiments.

Supplemental Figure 16



Supplemental Figure 16. *bsk1-1* showed wild type like MAP kinase activation, expression of PTI marker genes and seedling growth inhibition in response to flg22.

(A) MAPK activation in the *bsk1-1* seedlings by flg22 is similar to wild type. The seedlings of wild type, *bsk1-1* and *fls2* were treated with 100 nM flg22. The MAPK activity was detected by immunoblot analysis using anti- $p44/42$ -ERK antibody. The individual MAPK kinases are indicated by arrows (upper panel). Ponceau S staining of Rubisco is shown as a loading control (lower panel).

(B)-(D) Relative expression of three PTI marker genes after flg22 treatment. The seedlings were treated with 100 nM flg22, and the accumulation of transcripts of *At2g19190* (B), *At1g51890* (C) and *At2g17740* (D) at different time points was measured by quantitative real-time PCR. *ACTIN2* was used as the internal control. Bars are mean and standard deviation from three independent biological samples.

(E) Seedling growth inhibition triggered by flg22 in WT and *bsk1-1*. Five-day-old seedlings were treated with a relatively low concentration of flg22 for 10 days. The relative growth was documented by comparing fresh weights of treated seedlings with those of the untreated control. Data represent mean and standard deviation (n=12). The experiments were repeated at least three times with similar results.

Supplemental Table 1

List of Primers Used in this Study.

Primer name	Purpose	Sequence (5' to 3')
158g FP	complementation	GAGACAGCTCTTGTGTTCTTGAAA
158g RP	complementation	AAGTTGATGATAATGAAGCACCG
<i>bsk1-1d</i> CAPS-HaeIII FP	genotyping	GGTTATGGTTAAAGCCAGATTTG
<i>bsk1-1d</i> CAPS-HaeIII RP	genotyping	GCATAGTAAGTAGCATAGACTTGGC
BSK1-RNAi FP	RNAi construct	CATCTAGACTCGAGGCCTGCTCAAGAATGGATCTCAC
BSK1-RNAi RP	RNAi construct	CAAAGCTTGAATTCCTTCGAGCTGAGCTGCTTCGTTCC
BSK1-attB1	gateway cloning	GGGGACAAGTTTGTACAAAAAAGCAGGCTTCGAA GGAGATAGAACCATGGGTTGTTGTCAATCCTTGTTT
BSK1-attB2	gateway cloning	GGGGACCACTTTGTACAAGAAAGCTGGGTCAAGAT CCTCTGCCGCTCGTTGT
BSK1 G2A-attB1	gateway cloning	GGGGACAAGTTTGTACAAAAAAGCAGGCTTCGAA GGAGATAGAACCATGGCTTGTGTTGTCAATCCTTGTTT
FLS2-attB1	gateway cloning	GGGGACAAGTTTGTACAAAAAAGCAGGCTTCGAA GGAGATAGAACCATGAAGTTACTCTCAAAGACCTT
FLS2-attB2	gateway cloning	GGGGACCACTTTGTACAAGAAAGCTGGGTCAACTT CTCGATCCTCGTTACGAT
BAK1-attB1	gateway cloning	GGGGACAAGTTTGTACAAAAAAGCAGGCTTCGAA GGAGATAGAACCATGGAACGAAGATTAATGATCC
BAK1-attB2	gateway cloning	GGGGACCACTTTGTACAAGAAAGCTGG GTCTCTTGGACCCGAGGGGTATTC
pMAL-BSK1 FP	<i>in vitro</i> kinase assay	CTGGATCCATGGGTTGTTGTCAATCCTTGTT
pMAL-BSK1 RP	<i>in vitro</i> kinase assay	CTGAATTCTCAAGATCCTCTGCCGCTC
K104E FP	site-directed mutagenesis	CGTCGTTGGATCGCTGTCGAGAAGTTTACTAAGATGG
K104E RP	site-directed mutagenesis	CCATCTTAGTAAACTTCTCGACAGCGATCCAACGACG
S230A FP	site-directed mutagenesis	GGGATGGTAAAAGTTATGCCACAAATTTAGCTTATACAC
S230A RP	site-directed mutagenesis	GTGTATAAGCTAAATTTGTGGCATAACTTTTACCATCCC
BSK1-NP FP	GFP localization	CCTTAATTAAGAGACAGCTCTTGTGTTCTTGAAA
BSK1-NP RP	GFP localization	CTGAGCTCGAGAGAAAGAGTTGATAGTGGTCCG
BSK1-CDS FP	GFP localization	CTGAGCTCATGGGTTGTTGTCAATCCTTGTTT
BSK1-CDS RP	GFP localization	CTACCGGTAGAGATCCTCTGCCGCTCGTTGT
BSK1-RT FP	real-time PCR	GAGCCTCGAGAGAGACCAAATAC
BSK1-RT RP	real-time PCR	CCTCACCTAATGGCGAAAGTGG
PR1-RT FP	real-time PCR	TTCACAACCAGGCACGAGGAG
PR1-RT RP	real-time PCR	CTAACCCACATGTTACGGCG
PR2-RT FP	real-time PCR	GAATCAAGGAGCTTAGCCTCACC
PR2-RT RP	real-time PCR	GTAGAGCCGCATTTCGCTGGAT
PAD4-RT FP	real-time PCR	CTTTCTTCAGTTAAAGATCAAGGAAGG
PAD4-RT RP	real-time PCR	GGCAGAAGTTGTGTGCTAAACG
SID2-RTFP	real-time PCR	CGCAAGAAGTATGAGTCATGTTCCG
SID2-RT RP	real-time PCR	AACCTGTAACCGAACGACGC
FMO1-RT FP	real-time PCR	CTCTCTTCTGCGTGCCGTAGTT
FMO1-RTRP	real-time PCR	ATCCCTTTATCCGCTTCCTCAA
ACTIN2-RT FP	real-time PCR	TCTCCCGCTATGTATGTCCG
ACTIN2-RT RP	real-time PCR	GTCACGTCCAGCAAGGTCAAGA